Int. J. Nonlinear Anal. Appl.
Volume 12, Special Issue, Winter and Spring 2021, 2211-2222
ISSN: 2008-6822 (electronic)
http://dx.doi.org/10.22075/ijnaa.2021.6113

Numerical simulation of a power-law inelastic fluid in axisymmetric contraction by using a Taylor Galerkin-pressure correction finite element method

Alaa A. Sharhanl[a,*], Alaa H. Al-Muslimawi[a]

[a]*Department of Mathematics, College of Science, University of Basrah, Basrah, Iraq*

(Communicated by Madjid Eshaghi Gordji)

Abstract

In this investigation, shear-thinning and shear-thickening inelastic fluids through a contraction channel are presented based on a power-law inelastic model. In this regard, Navier–Stokes partial differential equations are used to describe the motion of fluids. These equations include a time-dependent continuity equation for the conservation of mass and time-dependent equations for the conservation of momentum. Numerically, a time-stepping Taylor Galerkin-pressure correction finite element method is used to treat the governing equations. A start-up of Poiseuille flow through axisymmetric 4:1 contraction channel for inelastic fluid are taken into consideration as instances to satisfy the method analysis. Here, the impacts of different parameters, such as Reynolds number (Re), the consistency parameter (k), and the power-law index (n), are examined. Mainly, the effect of these parameters on the convergence levels of solution components considering it the most important point of view. The findings demonstrate that the inelastic parameters have a significant influence on the rates of velocity and pressure temporal convergence, and this effect is observed significantly. Fundamentally, the rate of convergence for shear-thickening flow is found to be greater than of the convergence for shear-thinning flow. In addition, the critical level of Reynolds number is also determined for shear-thinning and shear-thickening situations. In this context, we captured that the critical level of Re for shear-thickening case is much higher than that found for shear-thinning case.

Keywords: Taylor Galerkin-pressure correction finite element method, Inelastic fluid, Viscosity, Power-law model

*Corresponding author
Email addresses: eala.khashab.sci@uobasrah.edu.iq (Alaa A. Sharhanl), alaa.abdullah@uobasrah.edu.iq (Alaa H. Al-Muslimawi)

Received: October 2021 *Accepted:* December 2021

1. Introduction

In recent years, numerical studies on flow differential equations with viscous properties have elicited considerable attention among scholars due to the highly nonlinear nature of these equations. Most recent studies are based on the finite element method, which adopts different formulations. Among these studies, numerical research on inelastic equations has been particularly successful and widely conducted using the finite element method. These inelastic equations are presented in the form of mass conservation, momentum partial differential equations and inelastic constitutive model [16]. The Taylor Galerkin-pressure correction (TG-PC) method, which presented firstly by Townsend and Webster [19] is one of the most popular formulations. Accordingly, this method is implemented to deal with Newtonian and non-Newtonian viscous incompressible flows. This method is consisted of two approaches: Taylor Galerkin and pressure correction methods. A two-step Lax–Wendroff time-stepping method is used in the former (predictor-corrector) that off prints in time via a Taylor series expansion [10, 14]. By contrast, the latter ensures second-order accuracy in time by broadening the incompressibility constraint [11, 1]. Thus, this method has elicited considerable attention with regard to treat different flow problems (for more details see [2, 11, 12, 18]). To reduce time errors in the time-stepping scheme, the algorithm used in the solution is based on the Crank–Nicolson method, which is given more accurate and good stability compared to others [30].

In the inelastic fluid the simplest basic constitutive equation is one that represents the viscous shear stress response as a power-law function is used to depict the shear-thinning and shear-thickening behavior of fluids. Such types of fluid were proposed by Ostwald–de Waele [4]. In power-law fluids, shear stress is related to shear rate ($\dot{\gamma}$).

$$\mu_s = k(\dot{\gamma})^{n-1}$$

where, k is a consistency parameter, and n is a power-law index. Higher k values in this model indicate that the fluid is more viscous. When $n = 1$, the Newtonian limiting approximation is obtained without shear rate dependence; when $n < 1$, shear thinning is observed, and when $n > 1$, shear thickening is seen [17]. Generally, the power-law fluids across the contraction of circular cylinders represent an idealization of many chemical and industrial processes encountered in polymers, minerals, foods, and biological industries. Thus, the present study is focused on the flow characteristics of power-law fluids across an axisymmetric contraction channel for a wide range of physical parameters such as, power-law index (n), consistency parameter (k) and Reynolds number (Re). The influences of these parameters on the behavior of fluid have been examined and reported herein. The main idea of the current study is to determine the temporal convergence-rate of the solution components that is taken to be steady state, which did not treat by authors before. For that purpose, Poiseuille() flow through axisymmetric contraction channel under isothermal condition has been conducted. Additionally, the study of inelastic fluid behavior by applying the TG-PC method with a constitutive power-law equation for a 4:1 contraction channel with an axisymmetric coordinate (r, z) is a new topic that has not yet been researched. We also determine the influence value changes of a consistency parameter (k), power-law index (n), and Reynolds number (Re) on the behavior of inelastic fluids. Furthermore, we identify the critical level of $Re(Re_{cri})$ and the relationship between critical $Re(Re_{cri})$ and the value of n in both cases shear thinning and shear thickening.

The mathematical modeling of non-Newtonian flow motion is presented in 2.1. The cylindrical coordinate system is used to introduce these equations. The numerical method is described in Section 2.2 since these equations must be investigated numerically. Sections 2.3 and 3 discuss the discretization of the problem and the numerical findings that resulted as a consequence of this discretization.

2. Methodology

2.1. Mathematical modeling

The forms of the continuity and momentum equations of incompressible inelastic flow under isothermal conditions when body forces are disregarded can be given as [16]:

$$\nabla \cdot u = 0 \tag{2.1}$$

$$\rho\left(\frac{\partial v}{\partial t} + u \cdot \nabla u\right) = -\nabla p + \nabla \cdot (2\mu_s(\dot{\gamma}, \dot{\varepsilon})d). \tag{2.2}$$

Where, u, ρ, p, and μ_s denote velocity, density, hydrodynamic pressure, and solvent viscosity, respectively. In addition, $d = \frac{1}{2}(\nabla u + \nabla u^{\tau})$ is the rate of the deformation tensor, and ∇ is the derivative operator (gradient). Furthermore, $\dot{\gamma}$ and $\dot{\varepsilon}$ represent the shear rate and strain rate of simple shear flow and extensional flow, respectively, such that

$$\begin{aligned} \dot{\gamma} &= 2\sqrt{II_d} \\ \dot{\varepsilon} &= 3\frac{III_d}{II_d} \end{aligned} \tag{2.3}$$

where, II_d and III_d represent the second and third invariants of the rate of strain tensor d, which can be defined in an axisymmetric coordinate system as follows [4]:

$$II_d = \frac{1}{2}\left\{\left(\frac{\partial u_r}{\partial r}\right)^2 + \left(\frac{\partial u_z}{\partial z}\right)^2 + \left(\frac{u_r}{r}\right)^2 + \frac{1}{2}\left(\frac{\partial u_r}{\partial z} + \frac{\partial u_z}{\partial r}\right)^2\right\}. \tag{2.4}$$

And

$$III_d = det\ (d) = \frac{u_r}{r}\left\{\frac{\partial u_r}{\partial r}\frac{\partial u_z}{\partial z} - \frac{1}{4}\left(\frac{\partial u_r}{\partial z} + \frac{\partial u_z}{\partial r}\right)^2\right\}. \tag{2.5}$$

In addition, the constitutive equation (Power Law Equation) is

$$\mu_s = k(\dot{\gamma})^{n-1}, \tag{2.6}$$

where, k is a consistency parameter and n is a power-law index.

In contrast, the equation can be also defined by the non-dimensional groups of Reynolds number (Re) by using the scaling $Re = \rho\frac{UL}{\mu}$, such that (U), (L) and (ρ) characteristic velocity, length and density, respectively. Thus, in this case, the non-dimensional form of the momentum equation in general Newtonian may be expressed as:

$$Re\left(\frac{\partial v}{\partial t} + u \cdot \nabla u\right) = -\nabla p + \nabla \cdot (2\mu_s(\dot{\gamma}, \dot{\varepsilon})d). \tag{2.7}$$

2.2. Numerical method

The Taylor Galerkin-pressure correction (TG-PC) method algorithm is a fractional step approach with three phases. In the first phase, u^* components are computed via a two-step predictor-corrector procedure by providing the initial velocity and pressure fields. In the second phase, pressure difference $(P^{n+1} - P^n)$ is evaluated by using u^* and applying the Choleski method. In the third phase, u^* and pressure difference $(P^{n+1} - P^n)$ are adopted to determine the velocity field u^{n+1} via Jacobi iteration.

Then the fractional step can be written as

$$\text{Stage 1a:}\frac{2Re}{\Delta t}[u^{n+\frac{1}{2}} - u^n] = L(u^n, d^n) - \nabla p^n, \tag{2.8}$$

$$\text{Stage 1b:}\frac{Re}{\Delta t}[u^* - u^n] = L(u^{n+\frac{1}{2}}, d^{n+\frac{1}{2}}) - \nabla p^n, \tag{2.9}$$

$$\text{Stage 2:}\nabla^2(p^{n+1} - p^n) = \frac{Re}{\theta\Delta t}\nabla \cdot u^*, \tag{2.10}$$

$$\text{Stage 3:}u^{n+1} = u^* - \frac{\theta\Delta t}{Re}[\nabla(p^{n+1} - p^n)]. \tag{2.11}$$

Where,

$$L(u, d) = [\nabla \cdot (2\mu_s(\dot{\gamma}, \dot{\varepsilon})d) - Re\ u \cdot \nabla u]. \tag{2.12}$$

Also, $\theta \in [0, 1]$, if choosing $\theta = \frac{1}{2}$ is chosen, the following technique is popular: the Crank–Nicolson scheme (a second-order temporal technique) and is referred to as the Crank–Nicolson parameter [8, 5].

It is possible to approximate velocity and pressure using the following formulas:

$$u(x, t) = \sum_{j=1}^{Ju} u_j(t)\phi_j(x), \tag{2.13}$$

$$p(x, t) = \sum_{j=1}^{Jp} p_j(t)\psi_j(x), \tag{2.14}$$

where, J_u indicates the total number of nodes, and J_p denotes the number of vertices of triangles. $u_j(t)$ and $p_j(t)$ represent the vector of velocity and pressure nodal values. The functions that serve as their foundation (shape or interpolation) are $\phi_j(x)$ and $\psi_j(x)$. u^* and pressure difference are represented by forms that are similar. The domain Ω is split into trigonometric elements., and the velocity at the mid-side and vertex nodes is calculated, whereas just the vertex nodes of a triangular are used to calculate pressure. Among the shape functions, $\phi_j(x)$ have been chosen as the quadratic basis function and $\psi_j(x)$ as the linear basis function Then, the corresponding TG-PC from Equations (2.8), (2.9), (2.10), and (2.11) may be written in matrix form as follows [11]).

$$\text{Stage 1a: } \left[\frac{2Re}{\Delta t}M + \frac{1}{2}S\right]\left(U^{n+\frac{1}{2}} - U^n\right) = \{-[S + Re\ N(U)]U + \mathcal{P}^T P\}^n, \tag{2.15}$$

$$\text{Stage 1b: } \left[\frac{Re}{\Delta t}M + \frac{1}{2}S\right](U^* - U^n) = \{-SU + \mathcal{P}^T P\}^n - Re[N(U)U]^{n+\frac{1}{2}}, \tag{2.16}$$

$$\text{Stage 2:}K(P^{n+1} - P^n) = -\frac{Re}{\theta\Delta t}\mathcal{P}U^*, \tag{2.17}$$

$$\text{Stage 3:}\frac{Re}{\theta\Delta t}M(U^{n+1} - U^*) = \theta\mathcal{P}^T(P^{n+1} - P^n), \tag{2.18}$$

where, U^n, U^{n+1} and P^n, P^{n+1} are nodal vectors of velocity and pressure at the time t^n and t^{n+1}, respectively; and U^* is an intermediate nodal velocity vector introduced in Step 1b. $M, S, N, \mathcal{P}$, and K respectively represent mass, momentum diffusion, convective, divergence/pressure gradient, and pressure stiffness matrices [9, 3, 15].

2.3. Problem specification and boundary conditions

The benchmark problem of flow through a 2D 4:1 axisymmetric sharp-corner contraction channel is selected for inelastic fluids under isothermal conditions in the current study. Accordingly, three different triangular finite element meshes, namely, fine mesh (MF), medium mesh (MM), and cross mesh (MC), are implemented, and diagrams for geometric configurations are provided in Fig. 1. The typical characteristics of finite element meshes are listed in Table 1.

Boundary conditions (BCs): The following is the BC setting for the current channel problem:

(a) The flow is defined as Poiseuille (Ps) flow with zero radial velocity at the inlet.

(b) No-slip BCs are put to the bottom walls of the channel.

(c) Slip BCs are applied to the axisymmetric line of the channel for axial velocity (u_z).

(d) The axisymmetric line has zero radial velocity, and zero pressure is applied at the channel's outlet.

Table 1: Parameters that affect the mesh

Mesh	Total Elements	Total Nodes	Boundary Nodes	Pressure Nodes
MF	1099	2318	239	610
MM	269	600	166	166
MC	121	282	81	81

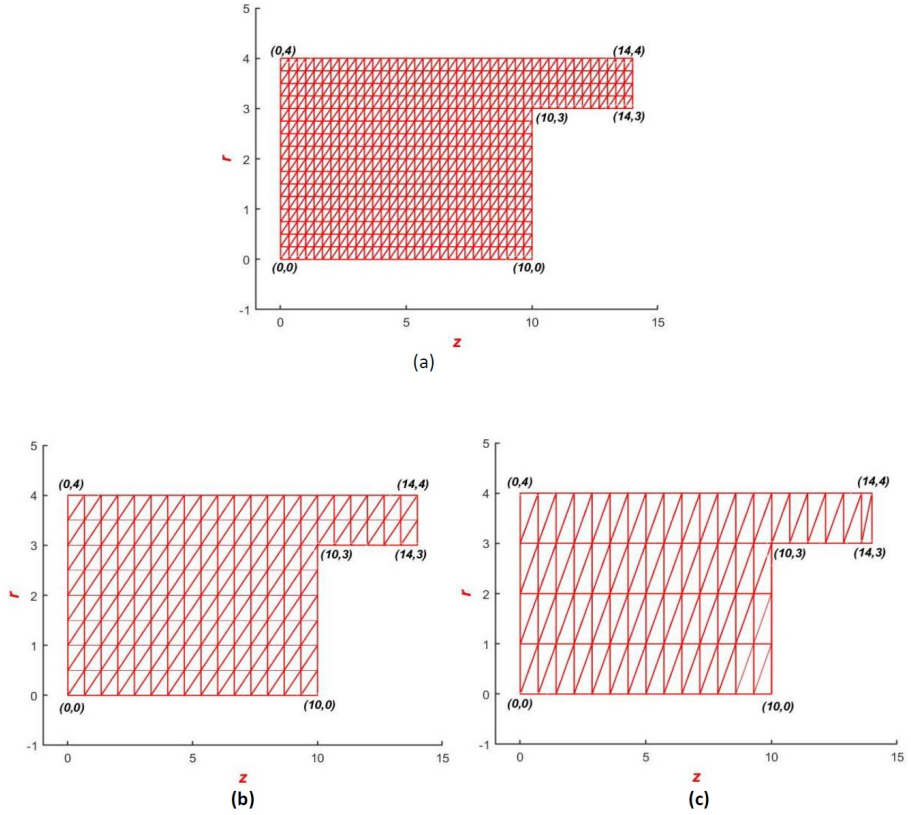

Figure 1: Structured finite element meshes (a) Fine mesh (b) Medium mesh (c) Cross mesh

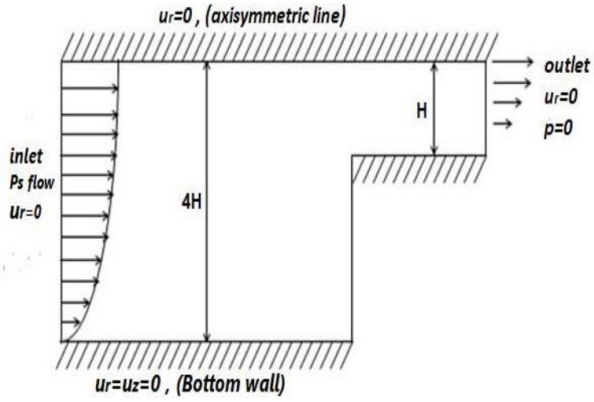

Figure 2: Flow geometry

3. Results

The Taylor Galerkin-pressure correction finite element method is utilized to solve the problem under consideration, and the numerical findings are concerned with the critical level of Reynolds number (Re_{cri}) and the rate of error convergence for the solution components. It is explored in this paper whether or not the parameters n, k, and Re have an impact on numerical convergence for inelastic flows via an axisymmetric 4:1 contraction channel by using three different meshes (CM, MM, and FM) (Fig. 1).

The critical level of Re is presented for FM, MM, and CM meshes in both shear thinning, ($n = 0.8$) and shear thickening, ($n = 1.8$) with fixed $k = 2$. The results shown that, a high (Re_{cri}) is observed for FM ($Re_{cri} = 2527$), while $Re_{cri} = 721$ for MM, and CM has a lower Re_{cri} (see Table 2). Thus, a conclusion can be drawn that different types of meshes provide varying outcomes [13], with a notable preference for FM. Accordingly, we use FM in the current study.

Table 2: Re_{cri} for three different meshes with $k = 2$

Mesh	Re_{cri} in shear thinning, ($n = 0.8$)	Re_{cri} in shear thickening, ($n = 1.8$)
CM	6	424
MM	17	721
FM	50	2527

In Fig. 3, Re_{cri} is illustrated as a function of n for the three meshes with $k = 2$. As indicated in the profiles, Re level increases as n increases with a high level has been seen for FM. In addition, the profile shows that the Re level for the shear-thickening case ($n > 1$) is higher than that for the shear-thinning case ($n < 1$). Additional comparative data are provided in Table 3.

n-variation: Fig. 4 shows the convergence rate for the axial velocity (u_z) component with different values of the power-law index (n), i.e., shear thinning ($n = 0.6, 0.8, 01$) and shear thickening ($n = 1.2, 2.8, 3$), with fixed $Re = 8$ and $k = 2$. In general the results reveal that, the level of convergence for velocity increases as the values of the power law index (n) are increasing for both cases of shear thinning and shear thickening. Here one can see that, the time step increases as the value of n increases, which is particularly apparent in the case of shear thickening. In addition,

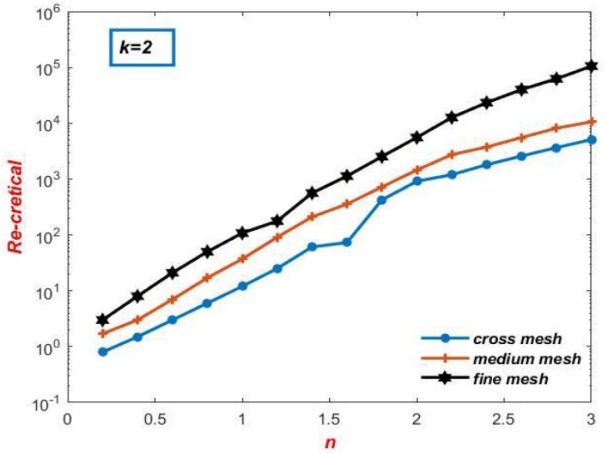

Figure 3: Relationship between Re_{cri} and type of mesh with $k = 2$ and $n = [0.2, 3]$

Table 3: Values of n with Re_{cri} maximum velocity, maximum pressure, and time step with $k = 2$

N	Re_{cri}	Maximum velocity	Maximum pressure	Time step
0.2	3	23.56	665.51	106
0.4	8	23.8	1667.15	75
0.6	21	24.1	4164.6	118
0.8	50	24.7	9785.8	104
1	108	25.3	21357.8	118
1.2	177	25	37547.7	55
1.4	562	26.3	107105	1239
1.6	1129	26.2	220955	995
1.8	2527	26.4	489769	883
2	5548	26.5	1.07187e+06	992
2.2	12650	26.4	2.41397e+06	3562
2.4	23312	26.3	4.69967e+06	1451
2.6	40002	26.02	8.5696e+06	2279
2.8	62354	25.4	1.42221e+07	2153
3	105007	25.01	2.48043e+07	7522

n-variation exerts no influence on velocity convergence in shear-thickening flows at beginning of the time, such that a minor shift at $(0 < Time-step < 15)$ is appeared as indicated in the zoomed section (see Fig 4b). Meanwhile, Fig. 5 shows a same feature at the convergence level of pressure under the same power-law index (n). In general for axial velocity and pressure, the rate of convergence for shear thickening requires more time steps compared to shear thinning. This finding is consistent with the results reported by Yasir et al., for shear thinning flows [20].

Fig. 6 illustrates the relationship between the maximum level of velocity at the top walls and the power-law index (n) in shear-thinning and shear-thickening cases, with $Re = 1$ and $k = 2$. From the profiles, one can see that the maximum velocity increases when n is increasing in both cases. Fig. 7 illustrates the criticial Re profile as a function of n at $k = 2$. The findings at the Re level demonstrate the influence of shear thinning and shear thickening on the critical level of Re. Here, it is seen that

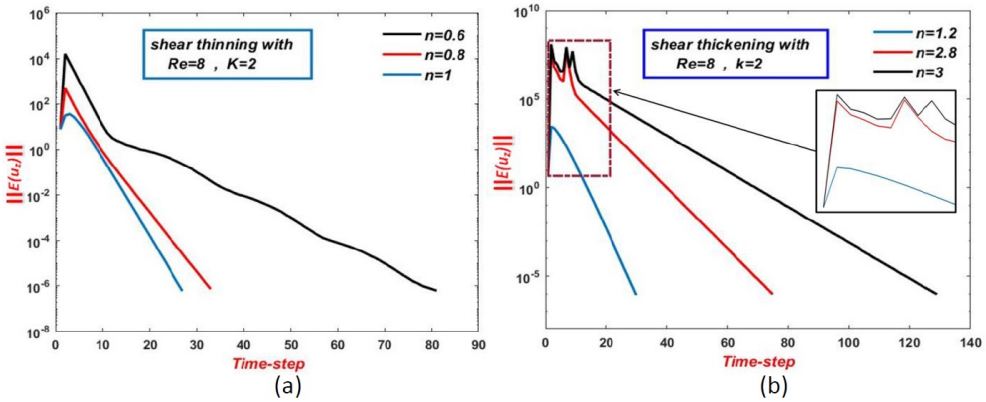

Figure 4: Convergence of velocity; n variation, $k = 2$, $Re = 8$, (a) shear thinning, (b) shear thickening

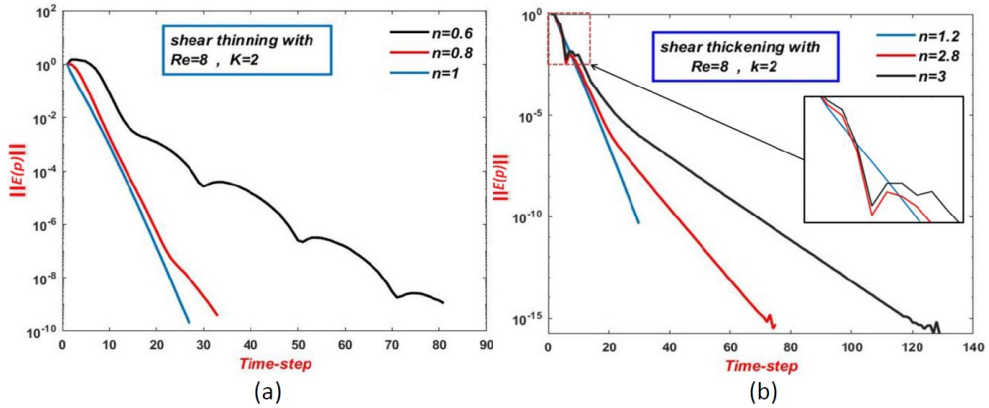

Figure 5: Convergence of pressure; n variation, $k = 2$, $Re = 8$, (a) shear thinning, (b) shear thickening

the level of Re decreases as the power law index (n) increases, so that the highest Re corresponds to the biggest power law index ($n = 3$). This finding is consistent with the results reported by Yasir et al., [20]; Coelho and Pinho [6, 7]; and Sivakumar et al. [17]. Fig. 8, explains that the Newtonian fluid has a lower time step than non-Newtonian fluid, and the time step increases when the power low index n drifts away from 1 to the left or right of it, implying that the Newtonian fluid requires less time step for convergence than non-Newtonian fluid.

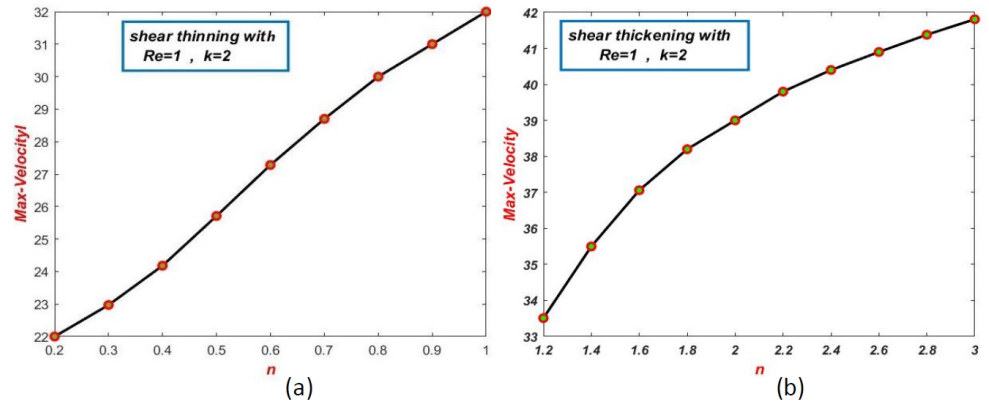

Figure 6: Increasing correlation between n and maximum velocity with $Re = 1$, $k = 2$, (a) shear thinning, (b) shear thickening

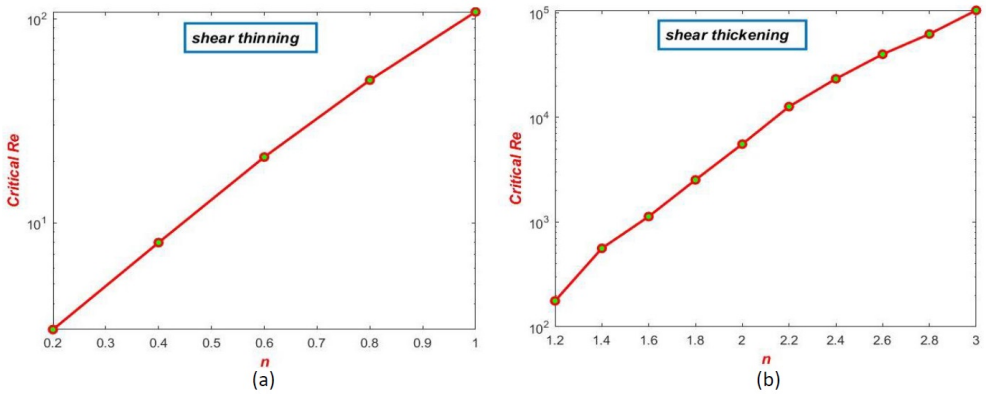

Figure 7: Re_{cri} vs. power law index n, (a) shear thinning, (a) shear thinning

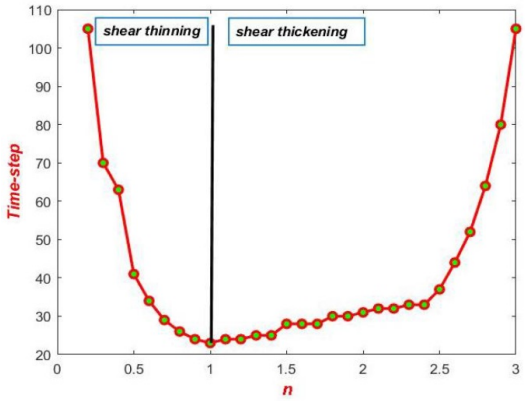

Figure 8: Power law index (n) vs. time step with $Re = 1$, $k = 2$

k-variation: Same features are observed of the effect of k-variation in both shear thinning case ($n = 0.8$) and shear thickening ($n = 2.8$) with fixed $Re = 10$. In this situation, the convergence level of axial velocity and pressure in the shear thinning and thickening flows is presented in Fig .9 and Fig. 10 to inspect the evolution of the solution with k variation. The results reveal that, for all values of k, the levels of convergence for velocity and pressure are virtually closed with gradually increasing as k-value decreased. This indicates that n has a higher influence on the behavior of fluid than k, and may be contrasted from (compare for example Fig. 4 and Fig. 9), which reflects a significant influence of viscous fluid characteristics on the level of convergence. Also, one can see that there is no effect at the beginning of the time ($0 < Time - step < 5$) for all solution components in both shear-thinning and shear-thickening flows (see the zoomed sections), which is consistent with the results reported by Yasir et al. [20].

Re-variation: Again the convergence of axial velocity for different Re in both shear thinning with $n = 0.8$ and $k = 2$ and shear thickening with $n = 1.2$ and $k = 2$ is illustrated in Fig. 11. From the profiles one can see that the level of time increments increases whenever you get increased in Re. For example when $Re = 2$, the level of time steps is much less than that in $Re = 20$, so the level of convergence of velocity is faster when Re is small. We note also that for the level of convergence in the shear thickening is almost double compared to the case of shear thinning, which reflects the difficulties of convergence for large Re number.

For same setting of parameters and flows, Fig. 12 illustrates the level of convergence for pressure components for various levels of Re. From the results, we observe that the level of pressure conver-

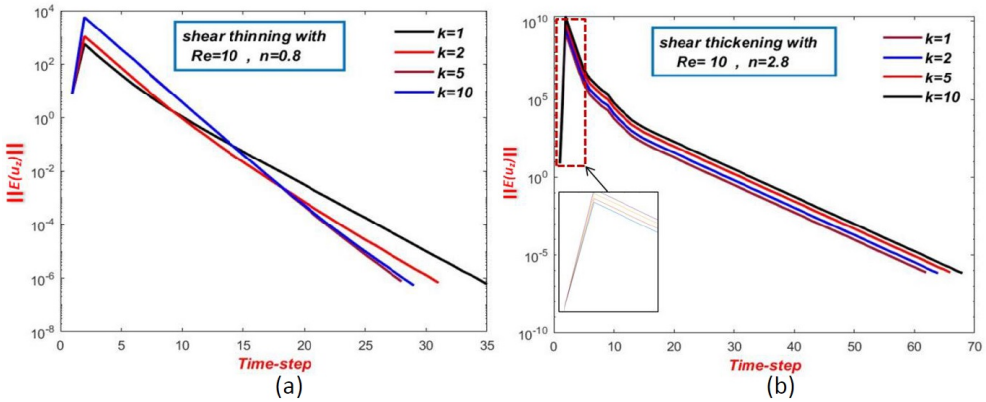

Figure 9: Convergence of velocity; k variation, (a) shear thinning, (b) shear thickening

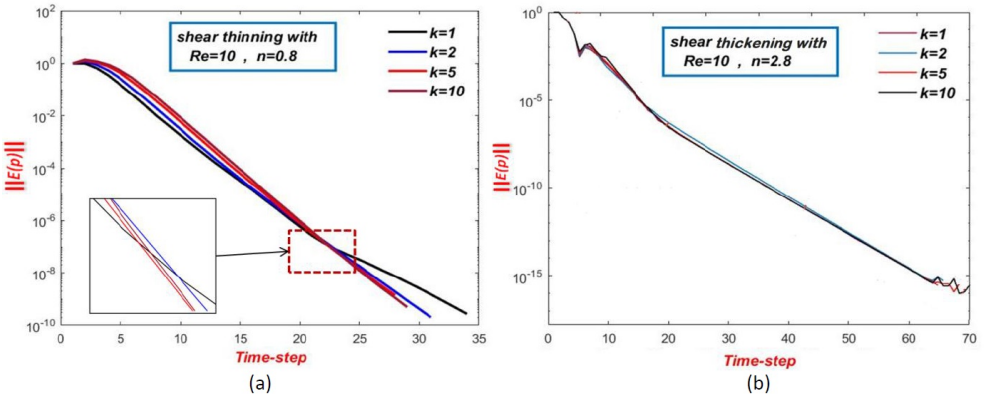

Figure 10: Convergence of pressure; k variation, (a) shear thinning, (b) shear thickening

gence increased as Re increased with modest change in shear thickening situation. This finding is consistent with the results reported by Yasir et al., for shear thinning flows [20].

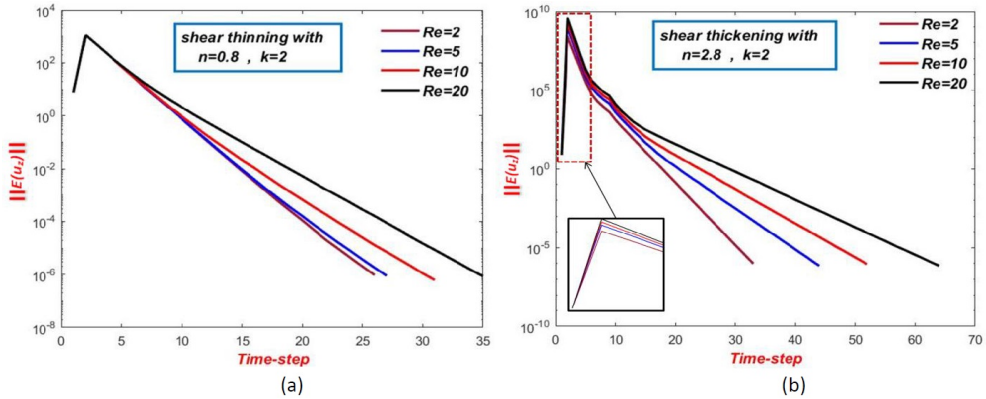

Figure 11: Velocity convergence, $k = 2$, Re variation, (a) shear thinning with $n = 0.8$, (b) shear thickening with $n = 1.2$

4. Conclusions

The Taylor Galerkin-pressure correction method is used to simulate an incompressible inelastic contraction flows in cylindrical coordinates system. The main ides of this study is to detect the effect

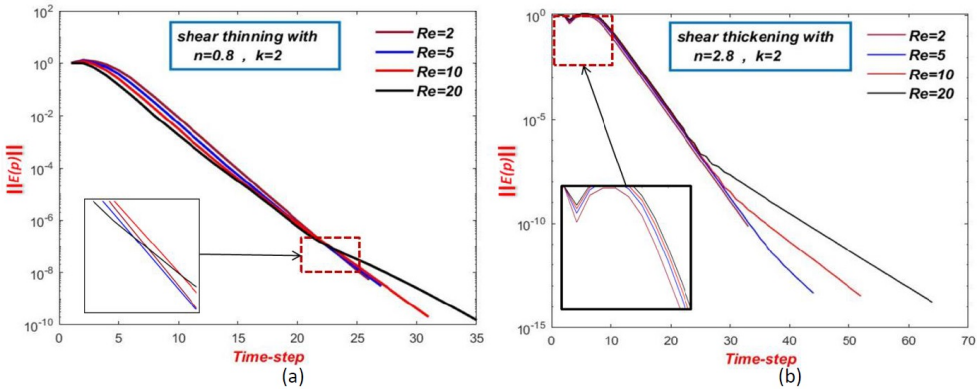

Figure 12: Pressure convergence, $k = 2$, Re variation, (a) shear thinning with $n = 0.8$, (b) shear thickening with $n = 1.2$

of the power law index (n), the consistency parameter (k), and the Reynolds number (Re) on the level of convergence in shear thinning and shear thickening cases. In addition, the critical Reynolds number for both cases of flow is investigated.

In this context, the rate of convergence of velocity and pressure increases as power-law index (n) rises in both cases of shear thinning and shear thickening. In addition, the rate of convergence in shear thickening flow is higher than that in shear thinning flow. Same feature is observed for k-variation and Re-variation. Moreover, impact of shear thinning and shear thickening behaviours on critical level of Re is provided as well. In this situation, we observed that the level of (Re) increases as increase in shear thinning and shear thickening tendency, which is agreement with experimental results and findings of others.

References

[1] M. Aboubacar, H. Matallah and M.F. Webster, *Highly elastic solutions for Oldroyd-B and Phan-Thien/Tanner fluids with a finite volume/element method: Planar contraction flows*, J. Non-Newtonian Fluid Mech. 103(1) (2002) 65–103.

[2] A. Al-Muslimawi, *Taylor Galerkin pressure correction (TGPC) finite element method for incompressible Newtonian cable-coating flows*, J. Kufa Math. Comput. 5(2) (2018) 14–22.

[3] A. Al-Muslimawi, H.R. Tamaddon-Jahromi and M.F. Webster, *Numerical simulation of tube-tooling cable-coating with polymer melts*, Korea-Aust. Rheol. J. 25(4) (2013) 197–216.

[4] F. Belblidia, T. Haroon and M.F. Webster, *The dynamics of compressible Herschel—Bulkley fluids in die-swell flows*, Boukharouba, M. Elboujdaini and G. Pluvinage (eds) Damage and Fracture Mechanics, Springer, Dordrecht, (2009) 425–434.

[5] C.-E. Bréhier, *Introduction to Numerical Methods for Ordinary Differential Equations*, Pristina, Kosovo, Serbia, 2016.

[6] P.M. Coelho and F.T. Pinho, *Vortex shedding in cylinder flow of shear-thinning fluids*, J. Non-Newtonian Fluid Mech. 110(2-3) (2003) 143–176.

[7] P.M. Coelho and F.T. Pinho, *Vortex shedding in cylinder flow of shear-thinning fluids III*, J. Non–Newtonian Fluid Mech. 121(1) (2004) 55–68.

[8] J. Crank and P. Nicolson, *A practical method for numerical evaluation of solutions of partial differential equations of the heat-conduction type*, Math. Proc. Camb. Phil.Soc. 43(1) (1947) 50–67.

[9] A.J. Davies, *The Finite Element Method: An Introduction With Partial Differential Equations*, OUP Oxford, 2011.

[10] J. Donea, *A Taylor-Galerkin method for convective transport problems*, Int. J. Numer. Meth. Eng. 20(1) (1984) 101–119.

[11] D.M. Hawken, H.R. Tamaddon-Jahromi, P. Townsend and M.F. Webster, *A Taylor-Galerkin-based algorithm for viscous incompressible flow*, Int. J. Numer. Meth. Fluids 10(3) (1990) 327–351.

[12] D.M. Hawken, P. Townsend and M.F. Webster, *Numerical simulation of viscous flows in channels with a step*, Comput. Fluids 20(1) (1991) 59–75.
[13] Y. Liu and G. Glass, *Effects of mesh density on finite element analysis*, SAE Tech. Paper 2013(1) (2013) 1375.
[14] R. Loehner, K. Morgan, J. Peraire and O. Zienkiewicz, *Finite element methods for high speed flows*, 7th Comput. Phys. Conf. 1985, pp. 1531.
[15] J.E. López-Aguilar, M.F. Webster, A.H.A. Al-Muslimawi, H.R. Tamaddon-Jahromi, R. Williams, K. Hawkins, C. Askill, C.L. Ch'ng, G. Davies, P. Ebden and K. Lewis, *A computational extensional rheology study of two biofluid systems*, Rheol. Acta 54(4) (2014) 287–305.
[16] G. Łukaszewicz and P. Kalita, *Navier–Stokes Equations An Introduction with Applications*, Springer International Publishing, 2018.
[17] P. Sivakumar, R.P. Bharti and R.P. Chhabra, *Effect of power-law index on critical parameters for power-law flow across an unconfined circular cylinder*, Chem. Eng. Sci. 61(18) (2006) 6035–6046.
[18] H.R. Tamaddon Jahromi, M.F. Webster and P.R. Williams, *Excess pressure drop and drag calculations for strain-hardening fluids with mild shear-thinning: Contraction and falling sphere problems*, J. Non-Newtonian Fluid Mech. 166(16) (2011) 939–950.
[19] P. Townsend and M.F. Webster, *An algorithm for the three-dimensional transient simulation of non-Newtonian fluid flows*, Proc. Int. Conf. Num. Meth. Eng.: Theory and Applications, NUMETA, Nijhoff, Dordrecht, 12 (1987) 123–133.
[20] R.Y. Yasir, Al.H. Al-Muslimawi and B.K. Jassim, *Numerical simulation of non-Newtonian inelastic flows in channel based on artificial compressibility method*, J. Appl. Comput. Mech. 6(2) (2020) 271–283.